Flash Freeze Flow Tube to Vitrify Aerosol Particles at Fixed Relative Humidity Values

Theresa M. Kucinski, Emily-Jean E. Ott, and Miriam Arak Freedman

Department of Chemistry, The Pennsylvania State University, University Park, PA 16801, USA

Revised Submission to *Analytical Chemistry*

March 4, 2020

* To Whom All Correspondence Should be Addressed: maf43@psu.edu, 814-867-4267

Abstract

Development of methods to measure the phase transitions and physical properties of submicron atmospheric aerosol particles is needed to better model these systems. In this paper, we present a method to flash freeze submicron particles to measure phase transitions as a function of relative humidity (RH). Particles are equilibrated at a fixed RH, vitrified in a temperature-controlled flow tube, and imaged with cryogenic transmission electron microscopy (cryo-TEM). We demonstrate the use of the technique for measuring the efflorescence relative humidity (ERH) of potassium sulfate and potassium chloride aerosol as well as the separation RH for a multicomponent organic/inorganic system that undergoes liquid-liquid phase separation (LLPS). The location of phase transitions can shift between the micrometer and nanometer size regimes and particles in a given population may have a range of RH over which a phase transition occurs. This technique addresses these requirements by allowing for characterization of the phase transitions for individual particles in a population on the submicron scale.

Introduction

Development of analytical techniques to characterize aerosol particles is crucial in understanding their effects on Earth's climate and weather. In The Future of Atmospheric Chemistry Research report, The National Academies of Sciences, Engineering, and Medicine lists "the development of analytical instrumentation, measurement platforms, laboratory, theory, and modeling capabilities" as part of the infrastructure needed to fulfil priority science areas.[1] Furthermore, they specify that the development of tools to understand composition, morphology, and phase need to progress over a broad size range from nanometer to micrometer size regimes.[1] While numerous studies of the physical properties of aerosol particles are performed on model micrometer particles, most aerosol particles in the atmosphere are in the submicron size regime. Characterization of particles in the nanoscale size regime is essential because they can have different properties from their bulk (micrometer) counterparts due to finite size and surface effects.[2–4] Literature shows that efflorescence and deliquescence occur at different relative humidity (RH) values on the nanoscale due to the Kelvin effect.[5,6] Additionally, particles do not always reach thermodynamic equilibrium due to processes such as diffusion, uptake, and changing temperature/pressure during transport/uplift that can create physical and chemical changes to aerosol. which leads to size dependence effects due to kinetics. Particles in the nanometer regime have been difficult to characterize due to limitations in available methods. To gain the best representation of the atmosphere, submicron particles need to be as well characterized as their micrometer counterpoints over a range of RH values, requiring development of new methodology. Particle morphology has been well documented on the micrometer scale with the use of optical microscopy that images aerosol particles over a range of RH values, along with several other characterization techniques such as FTIR and Raman.[7–11]

Accessing phase state information in relation to RH is essential for understanding the chemistry and physics of aerosol particles in the atmosphere. With cycling humidity levels in the atmosphere, aerosol particles can undergo efflorescence, deliquescence, and liquid-liquid phase separation (LLPS).[12,13] The resulting phase state can alter hygroscopic behavior, cloud condensation nuclei activity, reactive uptake, and several other properties that can affect aerosol impacts on climate.[8–11] Limiting phase state studies to the micrometer scale fails to account for the broad size range of atmospheric aerosol and nanoscale effects. For instance, nanometer sized particles that undergo LLPS have been shown to have a size-dependence, such that large particles phase separate and small particles remain homogenous.[18–20] Additionally, theory shows that efflorescence and deliquescence can differ on the nanometer scale due to particle size effects.[5,6]

Currently, there are several microscopy techniques employed to study submicron aerosol particles. Atomic force microscopy (AFM) has been used for analysis of atmospherically relevant particles.[21–23] Various types of electron microscopy (EM), such as environmental transmission electron microscopy (ETEM), are commonly used to study phase changes of submicron particles.[24,25] Transmission electron microscopy (TEM) in general provides information on morphology and size and is advantageous due to its ability to readily achieve images for large numbers of particles.[19–24] ETEM can be used to study phase transitions of aerosol particles by exposing particles on the TEM substrate to water vapor.[32] Similar to TEM, scanning electron microscopy (SEM), has also been used to study submicron aerosol particles.[33–36] In addition to the above techniques, scanning transmission x-ray microscopy with near edge X-ray absorption fine structure spectroscopy (STXM/NEXAFS) can resolve the organic/inorganic components in an internally mixed particle and can be used to study liquid-

liquid phase separation (LLPS) at high RH levels.[29,37,38] Note that in addition to microscopy techniques, hygroscopic tandem differential mobility analyzer (H-TDMA) analysis has been widely used to investigate efflorescence relative humidity (ERH) and deliquescence relative humidity (DRH) of submicron aerosol particles.[39] H-TDMA is used to measure ERH and DRH for ensembles of particles rather than individual particles.

In this study, we introduce a new method that allows for imaging of multicomponent submicron particles at specific RH with minimal damage using a vitrification flow tube. The system is based on the freeze-drying aerosol particles method published by Adler et al.[40] We have previously dried aerosol particles before collection and imaging, which avoids the use of a substrate during the phase transitions, but neglects critical information about the aqueous particle state.[19,20,26–28] Our new method vitrifies or "flash freezes" particles equilibrated at a chosen RH. Particles are subsequently imaged using cryogenic-TEM (cryo-TEM). Vitrification is a common technique in the biosciences that allows for TEM imaging of biological specimens with minimal damage.[41,42] It is an inexpensive cryopreservation technique used to preserve biological matter due to improved recovery of viable samples while retaining their initial morphology.[43–45] Vitrification freezes a cryopreservant (solvent) around a sample which immobilizes and maintains the solute structure thus creating a snapshot of a liquid locked in place.[41,46,47] The technique uses fast cooling rates that increase the viscosity of the system to the point that nucleation and crystal growth of water is hindered. The resulting phase is highly viscous and becomes a glass, which is a stable non-equilibrium phase.[48,49] Transitioning to the glassy state becomes easier to achieve in multicomponent systems due to solute molecules creating a structural barrier for ice formation.[49,50] The vitrified samples can then be imaged using cryogenic EM using a cold stage that permits imaging without dehydration and minimal damage.[41,51,52]

Aerosol particles can be similarly vitrified with the use of a temperature-controlled flow tube. Temperature-controlled flow tubes have been used previously to study particle freeze-drying, phase changes, as well as to measure freezing curves of aerosol droplets.[38,51] Our technique utilizes a temperature-controlled flow tube in combination with vitrification to produce a new technique to study nanometer particles over a range of RH values. Particles can be imaged at specific relative humidity points thus creating snapshots of the phase transition processes.

Experimental

Particle Generation and Drying

Aerosol particles are generated using an atomizer from a 0.05-0.07 wt% solution. A Tedlar bag (approximately 500 L) is filled with the generated particles (~98% RH). Particle count and RH is measured using a TSI condensation particle counter (CPC) model 3752 and Vaisala HMP110 RH and temperature probe. The probe has an uncertainty of ±1.5% RH. Particles are slowly dried (0.3-0.5% RH/minute) with ultra-purified N_2 (g). On average, the particle concentration ranges from $3x10^3$ to $1.4\ x10^4$ particles per cm^3. The size distributions of particles before and after vitrification is provided in Figure S1 of the Supporting Information

Flash Freeze Flow Tube

The flash freeze flow tube (Figure 1) consists of two concentric stainless-steel tubes.[40] Nitrogen gas is chilled through a copper coil submerged in liquid nitrogen and is flowed into the outer tube which acts as a jacket to cool the system. The system is covered with 1" flexible foam rubber insulation to maintain temperature throughout. Teflon tubing that can withstand temperatures down to -240 ^oC is used to transport particles to the flash freeze flow tube. Aerosol particles pass through the chilled inner tube at a port in the start of the flow tube. Particles, now vitrified, exit a second port at the end of the flow tube for collection. The flow rate exiting the

tube is $2.5x10^3$ sccm. The Reynold's number for the initial and final temperatures are both below $1x10^3$, indicating laminar flow throughout. The residence time of particles is approximately 0.9 seconds. The time needed for a particle of a given size to reach equilibrium at a given RH was calculated using the method from Chenyakin et al. and was on the order of several minutes.[54] In comparison, freezing occurs in less than a second. It is then reasonable to assume that the particles stay equilibrated to the bag surroundings with little to no change during freezing. The efflorescence relative humidity (ERH) of ammonium sulfate has been shown to stay approximately constant between 293 K and 233 K.[55] The ERH of citric acid/ammonium sulfate particles was also found to be approximately constant down to temperatures of 233 K for organic mass fractions of 0.1 and 0.15, but is temperature dependent below 250 K for higher organic mass fractions (0.20 and 0.25) .[55] Meanwhile, the ERH of palmitic acid and ammonium sulfate particles was insensitive to temperature changes down to 235 K.[56] Additionally, the separation relative humidity (SRH) for ten types of organic/ammonium sulfate particles has been shown to not be a strong function of temperature over a range of 244 to 290 K and varied less than 9.7% RH for all systems studied.[11]

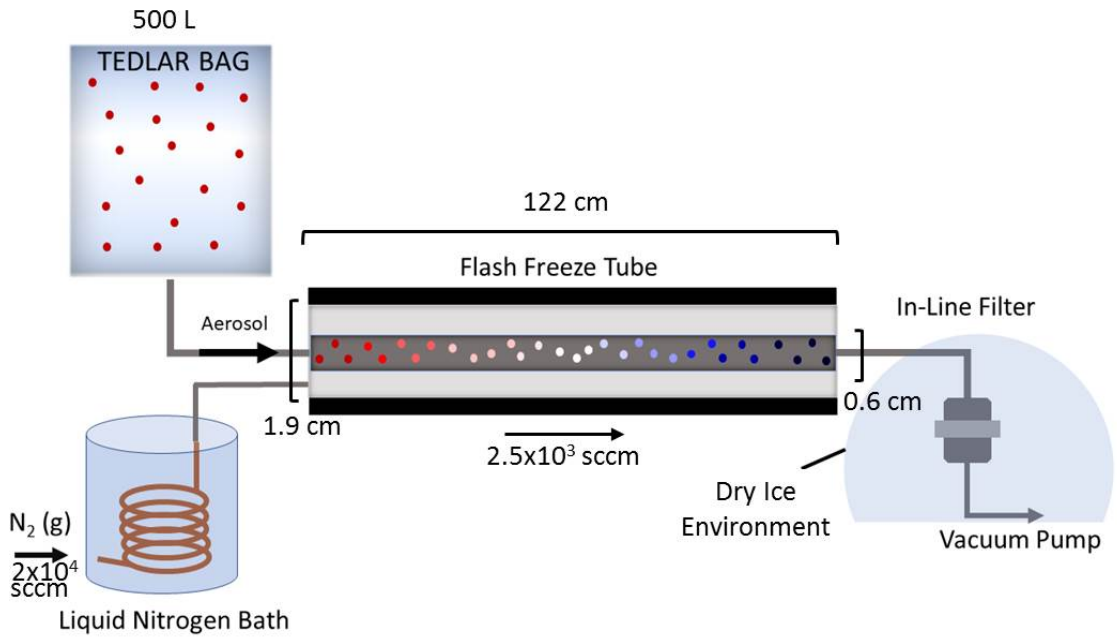

Figure 1. Schematic of the flash freeze technique. Aerosol particles are created with an atomizer that flows into the Tedlar bag where they are dried to a specific RH value. A vacuum pump pulls the particles through the flash freeze tube which has been cooled with chilled nitrogen gas. The vitrified particles are impacted onto a TEM grid using an in-line filter within a dry-ice environment.

A Sterlitech LS 25 Gas Line Holder (25mm, stainless steel) is used as an inline filter to collect vitrified particles onto copper TEM grids. The inline filter is contained in a dry ice environment that both chills at -78.5 ^{o}C and provides a CO_2 enriched environment to minimize water exposure. Particles reach the inline filter already vitrified, avoiding chance of acidification.

Imaging

TEM grids remain in the dry ice environment until transfer to a Gatan TEM cryo-holder. The cryo-holder is precooled using a cryo-transfer station and the grid is transferred in a liquid nitrogen environment. Imaging is performed at approximately -170 ^{o}C and 200 kV, at a spot size selected to avoid damage to the samples from the electron beam. The spot size, which is size of the beam on the sample, ranged from 4 to 6 (arb. units) for minimal damage and depended on the system. The cryogenic temperatures prevent the particles from damaging for tens of seconds while under the electron beam. Size information is gathered using the ImageJ software (NIH).

Theoretical Temperature and Cooling Rates

Temperature as a function of radius was determined by modeling conduction in one direction through multiple layers in cylindrical geometry assuming steady state conditions. The following equation was used to estimate the temperature throughout the radius of the flash freeze flow tube

$$T = T_1 + \frac{S}{4k}(R^2 - r^2)$$

where T is temperature at radial position r, T_1 is temperature at furthest radial point measured at the end of the flow tube, S is heat generation rate per unit volume dependent on material, k is thermal conductivity of the material, and R is the maximum radius.[57] The physical parameters are listed in Table S1 and a plot of temperature as a function of radius is in Figure S1 of the Supporting Information. The calculated temperature gradient shows that the outer tube, which contains the chilled nitrogen gas, has the lowest temperature of 218 K, and that temperature increases towards the center of the flow tube where it reaches 227 K. The outermost layer reaches the coldest temperature, and cools the internal components consisting of the stainless steel exterior and the nitrogen contained within the inner tube.

The cooling rate of individual particles in the flash freeze flow tube was calculated as a function of particle diameter. We applied the following equation, which describes cooling rate for falling particles in drop tube, to the particles in our system

$$\nu_c = \frac{6}{\rho C_p D}[\varepsilon_h \sigma_{SB}(Tpart^4 - T_o^4) + h(Tpart - T_o)]$$

where ν_c is the cooling rate, ρ is the density of the droplet, C_p is the specific heat, D is droplet diameter, ε_h is surface emissivity, σ_{SB} is the Stefan-Boltzmann constant, h is thermal transfer coefficient of the droplet, T_{part} is particle temperature, and T_o is the flash freeze temperature.[58,59]

Particle temperature is assumed to be equilibrated with ambient air temperatures prior to flash freezing. The flash freeze temperature refers to the temperature of the chilled nitrogen gas within the inner tube. Physical parameters of the particles were assumed to be equivalent to water and are listed in Table S1 of the Supporting Information. The cooling rate rapidly increases with decreasing particle diameter, as expected (Figure 2).[58] Particles will reach equilibrium with the flash freeze temperature within subnanoseconds to nanoseconds depending on particle diameter, producing vitrified particles.

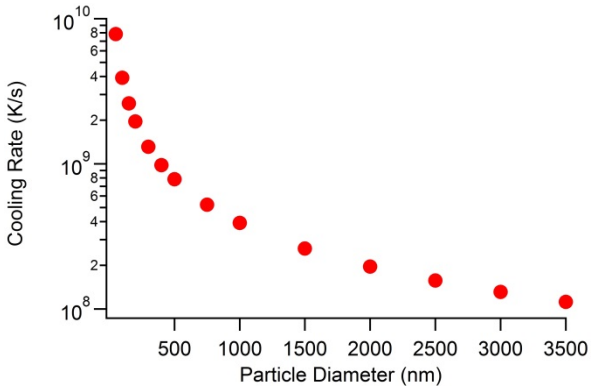

Figure 2. Calculated cooling rate (K/s) as a function of particle diameter. Smaller particles are expected to have a faster cooling rate compared to larger particles.

Results and Discussion

Imaging Efflorescence and Liquid-Liquid Phase Separation with Flash Freeze

The vitrification flow tube method was verified using two salts, potassium sulfate (K_2SO_4) and potassium chloride (KCl). Efflorescence and deliquescence of K_2SO_4 and KCl have been characterized for submicron particles previously using environmental TEM by Freney et al. and we verified RH by comparing to these previously published results.[44]

The characterization of these salts at the nanoscale is significant to this work due to the size dependence of efflorescence in inorganic salts. For instance, ERH of ammonium sulfate and sodium chloride decreased with decreasing dry particle size in particles as large as tens of

micrometers down to 50 nm.[60,61] Working in the same size regime as Freney et al.,[25] we were able to verify our method by measuring the ERH values for K_2SO_4 and KCl. Both systems were imaged above and just below efflorescence, in 2-3% RH increments. We found that the particles look empirically different prior to efflorescence compared to the effloresced salt. Above efflorescence, particles have low contrast, appearing as light grey (Figure 3). With decreasing RH, the contrast darkens, centralized at the core. Upon efflorescence, particles have high contrast appearing as a dark grey-black. At this point, reducing the electron beam onto the particle creates a diffraction pattern due to the crystal structure of the particle. Wise et al. identified the phase change of ammonium sulfate and potassium bromide using changes in particle diameters.[24] We compared the average particle sizes across RH levels and saw a decrease indicating the loss of water and ERH. The average particle size for KCl at 57% RH was $4x10^2 \pm 2x10^2$ nm and it decreased to $3x10^2 \pm 1x10^2$ nm at efflorescence (52% RH). Similarly, the average particle size for K_2SO_4 was $1.8x10^3 \pm 600$ nm at 68% RH and $1.6x10^2 \pm 50$ nm at efflorescence (61% RH). The provided average size is to give a sense of the amount of water loss, however, we must point out that each listed RH indicates a different experiment and does not track the same group of particles. K_2SO_4 and KCl particles have reported ERHs of 60±1% and 56±2% respectfully.[23] The experimental ERHs from this study are 61±3% and 52±4% RH for K_2SO_4 and KCl, respectfully. Studies show that ERH tends to decrease when transitioning between micrometer to submicron particles until approximately 40 nm when the Kelvin effect causes an increase in ERH.[55,57]

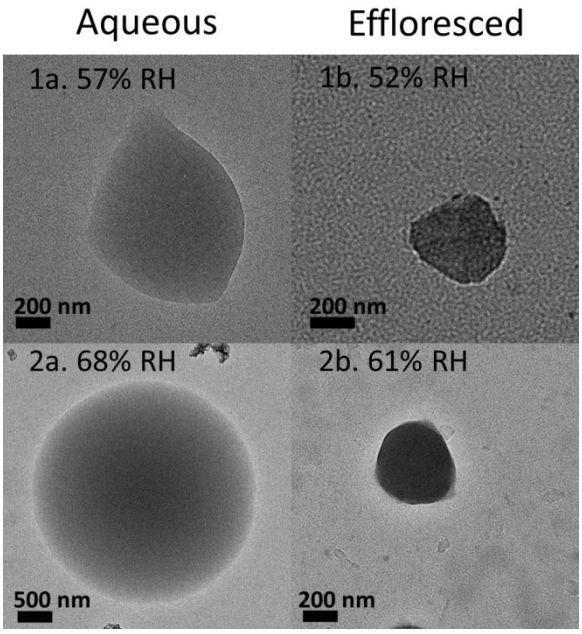

Figure 3. Progression of particle phase state for potassium chloride (1a-b) and potassium sulfate (2a-c) with RH. Potassium chloride effloresced at 52% RH (1b) and potassium sulfated effloresced at 61% RH (2c). The white halo around particles is due to under focusing the electron beam to produce optimal contrast.

Additionally, the vitrification flow tube can be used to determine the relative humidity at which liquid-liquid phase separation occurs. 2-Methylglutaric acid mixed with ammonium sulfate in a 2:1 ratio was imaged in approximately 5% RH increments as an example of the capabilities of this method to measure phase changes in multicomponent aerosol (Figure 4). Song et al. reports the SRH of 2:1 2-methylglutaric acid/ammonium sulfate as 75% RH for micrometer-sized particles.[63] 2-Methylglutaric acid/ammonium sulfate particles were imaged at several points above SRH until the RH at which LLPS was observed. Particles above SRH have light and uniform contrast showing no signs of phase separation. At the onset of SRH (65% RH for the particle in Figure 4) particles have a lighter contrast shell with a darker contrasted spherical core that indicates that phase separation has occurred. Core darkening with the appearance of a defined semi-circular core is the indication that the particle has undergone LLPS and is not present above SRH. Upon decreasing RH further (62% and 56% RH), phase separation becomes more defined with a decrease in overall average particle area and a

pronounced reduction in size of the outer shell indicating a decrease in water content. Particles are core shell at the onset of LLPS and progress to become partially engulfed with decreasing RH. This change in morphology has previously been observed with decreasing RH in micrometer diameter particles contained in an optical trap[64,65]

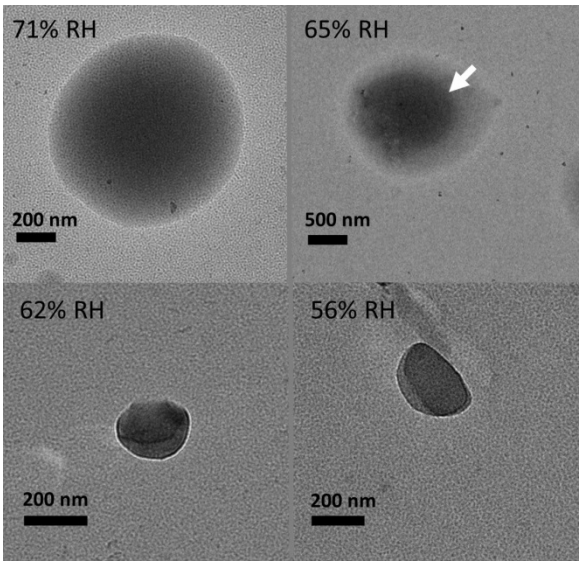

Figure 4. Progression of 2-methylglutaric acid (2-MGA) and ammonium sulfate (AS) particles with decreasing RH. At 71% RH, particles are uniform and have no clear indication of a secondary phase. At 65% RH, a new phase appears characterized by the distinct contrast difference (white arrow) indicating LLPS has occurred. At 62% and 56% RH, the morphology further develops.

We expect that SRH and ERH will be lower in submicron systems compared to supermicron droplets. Literature ERH values for inorganic salts including sodium chloride and ammonium sulfate are 5-15% lower for nanometer diameter particles compared to measurements of particles with micrometer diameters.[60,62] Additionally, the ERH and DRH of multicomponent particles have also been shown to change between 100 nm and 6 μm sized particles due to morphology.[62] We compared our flash freeze submicron ERH and SRH values to bulk values to determine size trends. Optical microscopy was used to determine the bulk ERH of K_2SO_4 and KCl.[9,66] From this study, we determined that K_2SO_4 has a bulk ERH of 73.3±5.4% RH and KCl has a bulk ERH of 65.3±3.5% RH (Table 1). These bulk values are significantly higher than previously published values for submicron to few micron diameter droplets that are listed in

Table 1.[25,67] From the flash freeze data, we see that ERH decreases more than 10% RH in submicron particles when compared to supermicron droplets (Table 1). Efflorescence occurs at approximately the same RH for most of the particles, and as a result, the size dependence of ERH cannot be assessed. Our lower overall submicron ERH values are consistent with previous results for inorganic salts and we expect that SRH will follow a similar trend. We compared submicron and bulk SRH values for 2-methylglutaric acid/ammonium sulfate (2:1). The published bulk SRH value for this system is 75.3±2.8% RH.[12] This study calculated submicron SRH by averaging the RH at which individual particles phase separate. The submicron SRH for 2-methylglutaric acid/ammonium sulfate (60±4% RH) is 12-15% RH lower than the reported values for micrometer-sized particles. A lower SRH for submicron systems could potentially impact future particle-resolved modeling when it accounts for the SRH of phase-separated particles.

Table 1. Efflorescence Relative Humidity (ERH) and Separation Relative Humidity (SRH) Values Compared to Literature

System	Particle Size	ERH (%)	Source
potassium sulfate	20-200 µm	73±5	This work
	~0.5-5 µm*	60±2	Freney et al.[25]
	100 nm – 2 µm	61±3	This work
potassium chloride	20-200 µm	65±4	This work
	~0.5-5 µm*	56±1	Freney et al.[25]
	20 µm	56	Cohen et al.[61]
	100-500 nm	52±4	This work
System	**Particle Size**	**SRH (%)**	**Source**
2-MGA/AS	28-34 µm	75.3±2.8	Song et al.[12]
	100 nm-1 µm	60±4	This work

* Particle size estimated from the scale bars in the TEM images provided by Freney et al.[25]

Limitations

Incorrect flash freeze preparation can be observed in cryo-TEM. Two possible errors in particle preparation are warming before imaging and not creating the correct cooling

environment to sufficiently flash freeze the particles. K_2SO_4 particles that were warmed after vitrification and cooled again for cryo-TEM show the wrinkled appearance (Figure 5a) compared to a K_2SO_4 particle that remained chilled throughout the duration of the experiment (Figure 5c). Cooling the flash freeze flow tube to the incorrect temperature or having the incorrect flow rate can lead to insufficient cooling rates. In this case, particles, especially those with large diameters, will not have completed the flash freeze process and remain somewhat fluid such that they rupture during impaction onto the TEM grids. A phase-separated 2-methylglutaric acid/ammonium sulfate particle in Figure 5b was prepared in a flash freeze flow tube that was insufficiently cooled. The arrow in Figure 5b indicates the region where the particle burst due to impaction. A vitrified phase-separated 2-methyl glutaric acid/ammonium sulfate particle shows no points of rupture and remains spherical (Figure 5d). Proper flow rates and post-vitrification handling methods can prevent these flash freeze preparation errors.

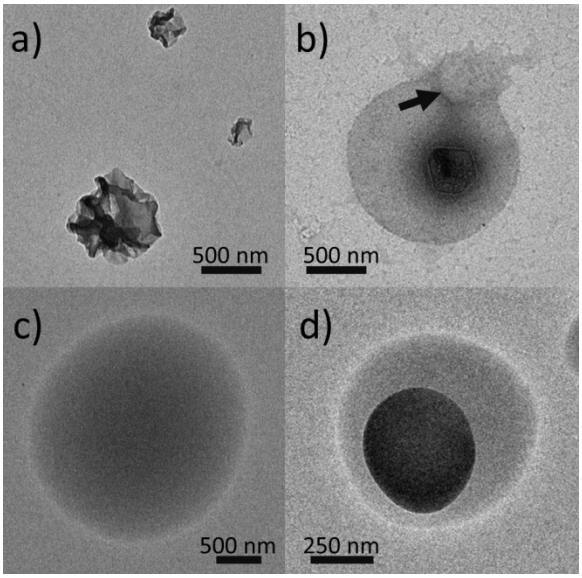

Figure 5. Example cryo-TEM images of particles with unsuccessful vitrification (top) and successful vitrification (bottom). Image a) shows potassium sulfate particles that have been vitrified and then warmed up prior to imaging in cryo-TEM and c) is a successfully vitrified particle that remained frozen the entire duration. Image b) is a phase separated particle that was prepared in an insufficiently cooled flash freeze flow tube causing it to rupture and d) is a successfully vitrified phase separated particle.

The flash freeze flow tube was constructed to be used in conjunction with cryo-TEM and is most suitable to image particles approximately 20 to $1x10^3$ nm in diameter. Particles are not expected to expand to the same degree as traditional freezing which produces crystallization. Vitrified water can be expected to expand by approximately 2% whereas frozen water can expand by approximately 10% of initial volume.[68–70] In the case of lower particle concentration, collection time will need to be increased which increases the risk of water contamination that can produce ice during cryo-TEM imaging. Phase state also affects imaging with cryo-TEM. Particles that have higher water content at the time of flash freezing appear with less contrast and require more underfocusing in the TEM, which creates the bright halo around the particle.

Conclusion

We describe the development of a vitrification flow tube that allows for the imaging of nanometer sized particles over a range of RH with the use of cryo-TEM. We verified the vitrification flow tube using potassium salts by comparing it to the results published previously that measured ERH of these systems on the submicron scale[25] Particles of 2-methylglutaric acid and ammonium sulfate were vitrified and imaged to showcase the practicality of this technique as a way to probe SRH for submicron multicomponent particles. This method proved to be successful in preparing particles to be imaged with cryo-TEM to capture efflorescence and LLPS. We anticipate the use of the vitrification flow tube technique as a way to gain further size-resolved information on the phase transitions of submicron aqueous particles and characterize LLPS at the submicron scale. This future work will parameterize submicron phase separation which can be used to improve particle-based models.

Acknowledgements

This research was supported by the U.S. Department of Energy, Office of Science, Basic Energy Sciences, Chemical Sciences, Geosciences, and Biosciences Division (DE-SC0018032).

Supporting Information Available: Size distribution of particles and physical parameters supplied as Supporting Information.

References

(1) National Academies of Sciences, Engineering, and Medicine. *The Future of Atmospheric Chemistry Research: Remembering Yesterday, Understanding Today, Anticipating Tomorrow*; The National Academies Press.: Washington, DC, 2016.
(2) Freedman, M. A. Phase Separation in Organic Aerosol. *Chem. Soc. Rev.* **2017**, *46*, 7694–7705.
(3) Biskos, G.; Russell, L. M.; Buseck, P. R.; Martin, S. T. Nanosize Effect on the Hygroscopic Growth Factor of Aerosol Particles. *Geophysical Research Letters* **2006**, *33*.
(4) Cheng, Y.; Su, H.; Koop, T.; Mikhailov, E.; Pöschl, U. Size Dependence of Phase Transitions in Aerosol Nanoparticles. *Nature Communications* **2015**, *6*.
(5) Biskos, G.; Malinowski, A.; Russell, L. M.; Buseck, P. R.; Martin, S. T. Nanosize Effect on the Deliquescence and the Efflorescence of Sodium Chloride Particles. *Aerosol Science and Technology* **2006**, *40* 97–106.
(6) McGraw, R.; Lewis, E. R. Deliquescence and Efflorescence of Small Particles. *The Journal of Chemical Physics* **2009**, *131*, 194705.
(7) Koop, T.; Ng, H. P.; Molina, L. T.; Molina, M. J. A New Optical Technique to Study Aerosol Phase Transitions: The Nucleation of Ice from H_2SO_4 Aerosols. *The Journal of Physical Chemistry A* **1998**, *102*, 8924–8931.
(8) Brooks, S. D. Phase Changes in Internally Mixed Maleic Acid/Ammonium Sulfate Aerosols. *Journal of Geophysical Research* **2003**, *108*.
(9) Losey, D. J.; Parker, R. G.; Freedman, M. A. PH Dependence of Liquid–Liquid Phase Separation in Organic Aerosol. *J. Phys. Chem. Lett.* **2016**, *7*, 3861–3865.
(10) Brunamonti, S.; Krieger, U. K.; Marcolli, C.; Peter, T. Redistribution of Black Carbon in Aerosol Particles Undergoing Liquid-Liquid Phase Separation. *Geophysical Research Letters* **2015**, *42*, 2532–2539.
(11) You, Y.; Bertram, A. K. Effects of Molecular Weight and Temperature on Liquid–Liquid Phase Separation in Particles Containing Organic Species and Inorganic Salts. *Atmospheric Chemistry and Physics* **2015**, *15*, 1351–1365.
(12) You, Y.; Smith, M. L.; Song, M.; Martin, S. T.; Bertram, A. K. Liquid–Liquid Phase Separation in Atmospherically Relevant Particles Consisting of Organic Species and Inorganic Salts. *International Reviews in Physical Chemistry* **2014**, *33*, 43–77.
(13) Freedman, M. A. Phase Separation in Organic Aerosol. *Chem. Soc. Rev.* **2017**, *46*, 7694–7705.
(14) Altaf, M. B.; Dutcher, D. D.; Raymond, T. M.; Freedman, M. A. Effect of Particle Morphology on Cloud Condensation Nuclei Activity. *ACS Earth Space Chem.* **2018**, *2*, 634–639.
(15) Zhang, Y.; Chen, Y.; Lambe, A. T.; Olson, N. E.; Lei, Z.; Craig, R. L.; Zhang, Z.; Gold, A.; Onasch, T. B.; Jayne, J. T.; et al. Effect of the Aerosol-Phase State on Secondary Organic Aerosol Formation from

the Reactive Uptake of Isoprene-Derived Epoxydiols (IEPOX). *Environmental Science & Technology Letters* **2018**, *5*, 167–174.

(16) Kuwata, M.; Martin, S. T. Phase of Atmospheric Secondary Organic Material Affects Its Reactivity. *PNAS* **2012**, *109*, 17354–17359.

(17) Hodas, N.; Zuend, A.; Schilling, K.; Berkemeier, T.; Shiraiwa, M. Discontinuities in Hygroscopic Growth Below and Above Water Saturation for Laboratory Surrogates of Oligomers in Organic Atmospheric Aerosols. 28.

(18) Veghte, D. P.; Altaf, M. B.; Freedman, M. A. Size Dependence of the Structure of Organic Aerosol. *J. Am. Chem. Soc.* **2013**, *135*, 16046–16049.

(19) Altaf, M. B.; Freedman, M. A. Effect of Drying Rate on Aerosol Particle Morphology. *J. Phys. Chem. Lett.* **2017**, *8*, 3613–3618.

(20) Kucinski, T. M.; Dawson, J. N.; Freedman, M. A. Size-Dependent Liquid–Liquid Phase Separation in Atmospherically Relevant Complex Systems. *J. Phys. Chem. Lett.* **2019**, *10*, 6915–6920.

(21) Bondy, A. L.; Kirpes, R. M.; Merzel, R. L.; Pratt, K. A.; Banaszak Holl, M. M.; Ault, A. P. Atomic Force Microscopy-Infrared Spectroscopy of Individual Atmospheric Aerosol Particles: Subdiffraction Limit Vibrational Spectroscopy and Morphological Analysis. *Anal. Chem.* **2017**, *89*, 8594–8598.

(22) Morris, H. S.; Grassian, V. H.; Tivanski, A. V. Humidity-Dependent Surface Tension Measurements of Individual Inorganic and Organic Submicrometre Liquid Particles. *Chem. Sci.* **2015**, *6*, 3242–3247.

(23) Morris, H. S.; Estillore, A. D.; Laskina, O.; Grassian, V. H.; Tivanski, A. V. Quantifying the Hygroscopic Growth of Individual Submicrometer Particles with Atomic Force Microscopy. *Anal. Chem.* **2016**, *88*, 3647–3654.

(24) Wise, M. E.; Biskos, G.; Martin, S. T.; Russell, L. M.; Buseck, P. R. Phase Transitions of Single Salt Particles Studied Using a Transmission Electron Microscope with an Environmental Cell. *Aerosol Science and Technology* **2005**, *39*, 849–856.

(25) Freney, E. J.; Martin, S. T.; Buseck, P. R. Deliquescence and Efflorescence of Potassium Salts Relevant to Biomass-Burning Aerosol Particles. *Aerosol Science and Technology* **2009**, *43*, 799–807.

(26) Veghte, D. P.; Bittner, D. R.; Freedman, M. A. Cryo-Transmission Electron Microscopy Imaging of the Morphology of Submicrometer Aerosol Containing Organic Acids and Ammonium Sulfate. *Anal. Chem.* **2014**, *86*, 2436–2442.

(27) Veghte, D. P.; Altaf, M. B.; Freedman, M. A. Size Dependence of the Structure of Organic Aerosol. *J. Am. Chem. Soc.* **2013**, *135*, 16046–16049.

(28) Bilal Altaf, M.; Zuend, A.; Arak Freedman, M. Role of Nucleation Mechanism on the Size Dependent Morphology of Organic Aerosol. *Chemical Communications* **2016**, *52*, 9220–9223.

(29) O'Brien, R. E.; Wang, B.; Kelly, S. T.; Lundt, N.; You, Y.; Bertram, A. K.; Leone, S. R.; Laskin, A.; Gilles, M. K. Liquid–Liquid Phase Separation in Aerosol Particles: Imaging at the Nanometer Scale. *Environ. Sci. Technol.* **2015**, *49*, 4995–5002.

(30) Li, J.; Anderson, J. R.; Buseck, P. R. TEM Study of Aerosol Particles from Clean and Polluted Marine Boundary Layers over the North Atlantic. *Journal of Geophysical Research: Atmospheres* **2003**, *108*.

(31) Adachi, K.; Chung, S. H.; Buseck, P. R. Shapes of Soot Aerosol Particles and Implications for Their Effects on Climate. *Journal of Geophysical Research: Atmospheres* **2010**, *115*.

(32) Ebert, M.; Inerle-Hof, M.; Weinbruch, S. Environmental Scanning Electron Microscopy as a New Technique to Determine the Hygroscopic Behaviour of Individual Aerosol Particles. *Atmospheric Environment* **2002**, *36*, 5909–5916.

(33) Johnson, K. S.; Zuberi, B.; Molina, L. T.; Molina, M. J.; Iedema, M. J.; Cowin, J. P.; Gaspar, D. J.; Wang, C.; Laskin, A. Processing of Soot in an Urban Environment: Case Study from the Mexico City Metropolitan Area. *Atmos. Chem. Phys.* **2005**, 11.

(34) Laskin, A.; Cowin, J. P.; Iedema, M. J. Analysis of Individual Environmental Particles Using Modern Methods of Electron Microscopy and X-Ray Microanalysis. *Journal of Electron Spectroscopy and Related Phenomena* **2006**, *150*, 260–274.

(35) A. Al-Hosney, H.; Carlos-Cuellar, S.; Baltrusaitis, J.; H. Grassian, V. Heterogeneous Uptake and Reactivity of Formic Acid on Calcium Carbonate Particles: A Knudsen Cell Reactor, FTIR and SEM Study. *Physical Chemistry Chemical Physics* **2005**, *7*, 3587–3595.

(36) Ault, A. P.; Peters, T. M.; Sawvel, E. J.; Casuccio, G. S.; Willis, R. D.; Norris, G. A.; Grassian, V. H. Single-Particle SEM-EDX Analysis of Iron-Containing Coarse Particulate Matter in an Urban Environment: Sources and Distribution of Iron within Cleveland, Ohio. *Environ. Sci. Technol.* **2012**, *46*, 4331–4339

(37) Laskin, A.; Moffet, R. C.; Gilles, M. K.; Fast, J. D.; Zaveri, R. A.; Wang, B.; Nigge, P.; Shutthanandan, J. Tropospheric Chemistry of Internally Mixed Sea Salt and Organic Particles: Surprising Reactivity of NaCl with Weak Organic Acids. *Journal of Geophysical Research: Atmospheres* **2012**, *117*. https://doi.org/10.1029/2012JD017743. Moffet, R. C.; Henn, T.; Laskin, A.; Gilles, M. K. Automated Chemical Analysis of Internally Mixed Aerosol Particles Using X-Ray Spectromicroscopy at the Carbon K-Edge †. *Analytical Chemistry* **2010**, *82*, 7906–7914.

(39) Swietlicki, E.; Hansson, H.-C.; Hämeri, K.; Svenningsson, B.; Massling, A.; Mcfiggans, G.; Mcmurry, P. H.; Petäjä, T.; Tunved, P.; Gysel, M.; et al. Hygroscopic Properties of Submicrometer Atmospheric Aerosol Particles Measured with H-TDMA Instruments in Various Environments—a Review. *Tellus B: Chemical and Physical Meteorology* **2008**, *60*, 432–469.

(40) Adler, G.; Koop, T.; Haspel, C.; Taraniuk, I.; Moise, T.; Koren, I.; Heiblum, R. H.; Rudich, Y. Formation of Highly Porous Aerosol Particles by Atmospheric Freeze-Drying in Ice Clouds. *PNAS* **2013**, *110*, 20414–20419.

(41) Dubochet, J.; McDowall, A. W. Vitrification of Pure Water for Electron Microscopy. *Journal of Microscopy* **1981**, *124*, 3–4.

(42) Hurbain, I.; Sachse, M. The Future Is Cold: Cryo-Preparation Methods for Transmission Electron Microscopy of Cells. *Biology of the Cell* **2011**, *103*, 405–420.

(43) Dhali, A.; Manik, R. S.; Das, S. K.; Singla, S. K.; Palta, P. Verification of Buffalo (Bubalus Bubalisi) Oocytes. *Theriogenology* **2000**, *53*, 1295–1303.

(44) Stachecki, J. J.; Garrisi, J.; Sabino, S.; Caetano, J. P.; Wiemer, K. E.; Cohen, J. A New Safe, Simple and Successful Vitrification Method for Bovine and Human Blastocysts. *Reproductive BioMedicine Online* **2008**, *17*, 360–367.

(45) Mahmoudzadeh, A. R.; Van Soom, A.; Ysebaert, M. T.; de Kruif, A. Comparison of Two-Step Vitrification versus Controlled Freezing on Survival of in Vitro Produced Cattle Embryos. *Theriogenology* **1994**, *42*, 1389–1397.

(46) Dubochet, J. Cryo-EM—the First Thirty Years. *Journal of Microscopy* **2012**, *245*, 221–224.

(47) Won, Y.-Y. Imaging Nanostructured Fluids Using Cryo-TEM. *Korean J. Chem. Eng.* **2004**, *21*, 296–302.

(48) Angell, C. A. Liquid Fragility and the Glass Transition in Water and Aqueous Solutions. *Chem. Rev.* **2002**, *102*, 2627–2650.

(49) Wolfe, J.; Bryant, G. Freezing, Drying, and/or Vitrification of Membrane– Solute–Water Systems. *Cryobiology* **1999**, *39*, 103–129.

(50) Zhang, W.; Yang, G.; Zhang, A.; Xu, L. X.; He, X. Preferential Vitrification of Water in Small Alginate Microcapsules Significantly Augments Cell Cryopreservation by Vitrification. *Biomed Microdevices* **2010**, *12*, 89–96.

(51) Jackson, C. L.; Chanzy, H. D.; Booy, F. P.; Drake, B. J.; Tomalia, D. A.; Bauer, B. J.; Amis, E. J. Visualization of Dendrimer Molecules by Transmission Electron Microscopy (TEM): Staining Methods and Cryo-TEM of Vitrified Solutions. *Macromolecules* **1998**, *31*, 6259–6265.
(52) Cheng, Y.; Grigorieff, N.; Penczek, P. A.; Walz, T. A Primer to Single-Particle Cryo-Electron Microscopy. *Cell* **2015**, *161*, 438–449.
(53) Bertram, A. K.; Patterson, D. D.; Sloan, J. J. Mechanisms and Temperatures for the Freezing of Sulfuric Acid Aerosols Measured by FTIR Extinction Spectroscopy. *J. Phys. Chem.* **1996**, *100*, 2376–2383.
(54) Chenyakin, Y.; Ullmann, D. A.; Evoy, E.; Renbaum-Wolff, L.; Kamal, S.; Bertram, A. K. Diffusion Coefficients of Organic Molecules in Sucrose–Water Solutions and Comparison with Stokes–Einstein Predictions. *Atmospheric Chemistry and Physics* **2017**, *17*, 2423–2435.
(55) Bodsworth, A.; Zobrist, B.; K. Bertram, A. Inhibition of Efflorescence in Mixed Organic–Inorganic Particles at Temperatures Less than 250 K. *Physical Chemistry Chemical Physics* **2010**, *12*, 12259–12266.
(56) Wise, M. E.; Baustian, K. J.; Tolbert, M. A. Internally Mixed Sulfate and Organic Particles as Potential Ice Nuclei in the Tropical Tropopause Region. *PNAS* **2010**, *107*, 6693–6698.
(57) Venkanna, B. K. *Fundamentals of Heat and Mass Transfer*; PHI Learning Pvt. Ltd., 2010.
(58) Dai, F.; Cao, C.; Wei, B. Phase Separation and Rapid Solidification of Liquid Cu60Fe30Co10 Ternary Peritectic Alloy. *SCI CHINA SER G* **2007**, *50*, 509–518.
(59) Adkins, N. J. E.; Tsakiropoulos, P. Design of Powder Metallurgy Aluminium Alloys for Applications at Elevated Temperatures Part 1 Microstructure of High Pressure Gas Atomized Powders. *Materials Science and Technology* **1991**, *7*, 334–340.
(60) Gao, Y.; Chen, S. B.; Yu, L. E. Efflorescence Relative Humidity for Ammonium Sulfate Particles. *The Journal of Physical Chemistry A* **2006**, *110*, 7602–7608.
(61) Gao, Y.; Chen, S. B.; Yu, L. E. Efflorescence Relative Humidity of Airborne Sodium Chloride Particles: A Theoretical Investigation. *Atmospheric Environment* **2007**, *41*, 2019–2023.
(62) Laskina, O.; Morris, H. S.; Grandquist, J. R.; Qin, Z.; Stone, E. A.; Tivanski, A. V.; Grassian, V. H. Size Matters in the Water Uptake and Hygroscopic Growth of Atmospherically Relevant Multicomponent Aerosol Particles. *J. Phys. Chem. A* **2015**, *119*, 4489–4497.
(63) You, Y.; Renbaum-Wolff, L.; Bertram, A. K. Liquid–Liquid Phase Separation in Particles Containing Organics Mixed with Ammonium Sulfate, Ammonium Bisulfate, Ammonium Nitrate or Sodium Chloride. *Atmospheric Chemistry and Physics* **2013**, *13*, 11723–11734.
(64) Stewart, D. J.; Cai, C.; Nayler, J.; Preston, T. C.; Reid, J. P.; Krieger, U. K.; Marcolli, C.; Zhang, Y. H. Liquid–Liquid Phase Separation in Mixed Organic/Inorganic Single Aqueous Aerosol Droplets. *J. Phys. Chem. A* **2015**, *119*, 4177–4190.
(65) Gorkowski, K.; Donahue, N. M.; Sullivan, R. C. Emulsified and Liquid–Liquid Phase-Separated States of α-Pinene Secondary Organic Aerosol Determined Using Aerosol Optical Tweezers. *Environ. Sci. Technol.* **2017**, *51*, 12154–12163.
(66) Losey, D. J.; Parker, R. G.; Freedman, M. A. PH Dependence of Liquid–Liquid Phase Separation in Organic Aerosol. *J. Phys. Chem. Lett.* **2016**, *7*, 3861–3865.
(67) Cohen, M. D.; Flagan, R. C.; Seinfeld, J. H. Studies of Concentrated Electrolyte Solutions Using the Electrodynamic Balance. 1. Water Activities for Single-Electrolyte Solutions. *J. Phys. Chem.* **1987**, *91*, 4563–4574.
(68) Leapman, R. D.; Sun, S. Cryo-Electron Energy Loss Spectroscopy: Observations on Vitrified Hydrated Specimens and Radiation Damage. *Ultramicroscopy* **1995**, *59*, 71–79.
(69) Adrian, M.; Dubochet, J.; Lepault, J.; McDowall, A. W. Cryo-Electron Microscopy of Viruses. *Nature* **1984**, *308*, 32–36.

(70) United States. Dept. of Commerce. Office of Technical Services. *Refrigeration Engineering*; U.S. Office of Technical Services., 1939.

For TOC Only